Transient Absorption Microscopy of Layered Crystal AsSbS₃

Pengzhi Wang,[†] Dawei He,[†] Jiaqi He,[‡] Jialu Fu,[†] Shuangyan Liu,[†] Xiuxiu Han,[†]
Yongsheng Wang,^{*,†} and Hui Zhao^{*,¶}

†Key Laboratory of Luminescence and Optical Information, Ministry of Education,
Institute of Optoelectronic Technology, Beijing Jiaotong University, Beijing 100044, China
‡College of Mathematics and Physics, Beijing University of Chemical Technology, Beijing
100029, China

¶Department of Physics and Astronomy, The University of Kansas, Lawrence, Kansas
66045, United States

E-mail: yshwang@bjtu.edu.cn; huizhao@ku.edu

Abstract

We introduce getchellite as a new layered material for fabrication of two-dimensional van der Waals materials and heterostructures. Nanofilms of $AsSbS_3$ were fabricated by mechanical exfoliation. Transient absorption spectroscopy measurements identified a direct bandgap at about 710 nm, which is close to the ideal single-junction photovoltaic bandgap. Transient absorption microscopy measurements with high spatial and temporal resolution were performed to reveal the spatiotemporal dynamics of photocarriers in $AsSbS_3$. We obtained a photocarrier lifetime of about 200 ps, a diffusion coefficient of about 5 cm² s⁻¹, a diffusion length of about 320 nm, and a carrier mobility of about 200 cm² V⁻¹ s⁻¹. These results establish $AsSbS_3$ as a promising two-dimensional semiconductor for optoelectronic applications as an individual material or in heterostructures.

INTRODUCTION

The discovery of graphene^{1,2} has created an exponentially growing interest in layered materials from which two-dimensional (2D) materials can be fabricated.^{3,4} So far, the most profound examples⁵ include layered transition metal dichalcogenides, transition metal oxides, hexagonal boron nitride, and black phosphorus, etc. Due to their atomic thinness, 2D materials made from layered crystals possess several unique features, such as thickness-dependent electronic structures^{6–8} and crystalline symmetry, ^{9–13} reduced dielectric screening, ^{14–16} and near-perfect surfaces without dangling bonds. ¹⁷ These features make 2D materials attractive candidates for electronic and optoelectronic applications. ^{18–23} Furthermore, these 2D materials provide a new route to fabricating heterostructures²⁴ by combining them via van der Waals interlayer interaction. Since lattice match is no longer a constraint, a large number of materials can be chosen from to assemble multilayers with certain properties. Hence, this new approach can produce a vast number of new materials for many applications, and can potentially transform material discovery. ^{25,26}

One important research direction in 2D materials is to identify new layered crystals with novel electronic or optical properties. Newly discovered layered crystals can enrich the material library to produce 2D materials and, more importantly, 2D heterostructures. A recent first-principles survey of materials has revealed that there exist more than 5000 layered crystals, ²⁷ with about one third of which are exfoliable. Therefore, despite of extensive efforts in the last decade on 2D materials, there are still a large number of materials to be explored.

In this article, we introduce a new type of layered semiconductor, getchellite, to the 2D research. Getchellite has been known as an antimony sulfide mineral for several decades. ²⁸ With the molecular formula of AsSbS₃, getchellite is a monoclinic layered crystal. This crystalline structure is similar to CuTeO₃, ²⁹ a predicted nodal-loop semimetal. ³⁰ The monoclinic structure also exists in commonly known 2D materials, such as MoTe₂. ^{31,32} By transient absorption microscopic and spectroscopic measurements, we identified a direct bandgap of about 1.74 eV in bulk AsSbS₃ at room temperature. By spatially and temporally resolving a differential reflection associated with this transition, we obtained a photocarrier lifetime of about 200 ps and an in-plane photocarrier diffusion coefficient of about 5 cm² s⁻¹. These results provide fundamental information for understanding photocarriers in this new material and its potential optoelectronic applications.

EXPERIMENTAL METHODS

The photocarrier dynamics in AsSbS₃ was studied by using a homemade transient absorption microscopy setup, which is schematically shown in Figure 1. The femtosecond laser system is composed of an 80-MHz passively modelocked Ti:sapphire laser and an optical parametric oscillator (OPO). The Ti:sapphire laser produces 100-fs pulses with a central wavelength of 820 nm, the majority of which is used to pump the OPO. The signal output of the OPO at about 712 nm was used as the probe pulse. The rest of the 820 nm pulse was incident to a beta barium borate (BBO) crystal to generate its second harmonic at 410 nm, which

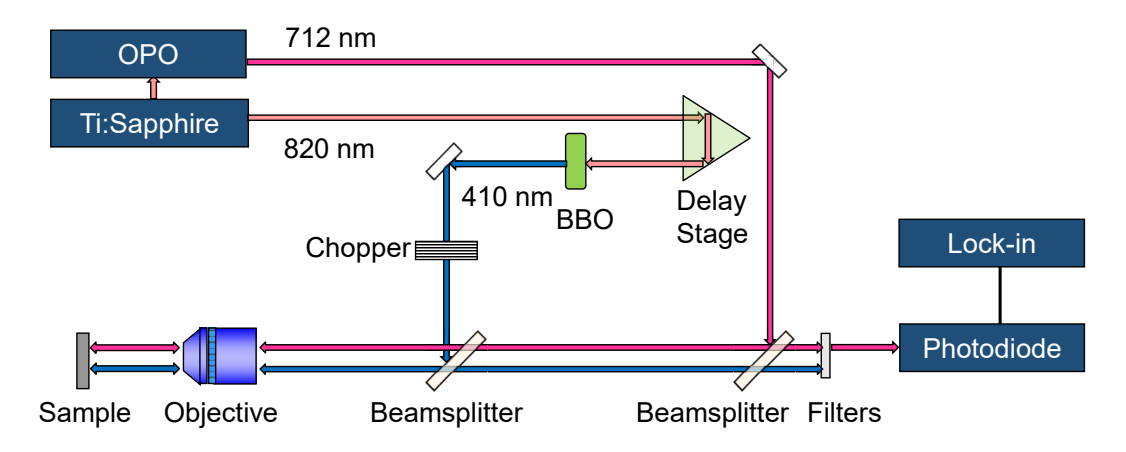


Figure 1: Schematics of the transient absorption microscope setup.

was used as the pump pulse. The pump and the probe each goes through a half-wave plate and a polarizer to control their polarization and power. They were then combined with a beamsplitter and focused to the sample through a microscope objective lens with a numerical aperture of 0.4. The sizes of the pump and probe spots at sample are about 1.8 and 2.3 μ m in full width at half maximum, respectively, determined by using an imaging system (not shown). The reflected probe beam was sent to a silicon photodiode, which output was measured by a lock-in amplifier. A series of filters were used in front of the photodiode to block the reflected pump beam. A mechanical chopper was used in the pump arm to modulate the pump intensity at about 2 kHz, which was synchronized with the lock-in amplifier.

We used differential reflection to probe the photocarrier dynamics. The differential reflection is defined as $\Delta R/R_0 = (R-R_0)/R_0$, where R and R_0 are the reflection coefficients of the sample with and without the presence of the pump, respectively. This quantity reflects the change of the complex index of refraction of the sample at the probe wavelength induced by the photocarriers injected by the pump. ³³ Hence, the spatiotemporal evolution of this signal after the pump excitation monitors the dynamics of the photocarriers injected by the pump. The differential reflection signal can be measured as a function of the probe delay, which is defined as the arrival time of the probe pulse at sample with respect to the pump pulse. This is achieved by using a retroreflector in the pump arm that is installed

on a motorized linear stage. The differential reflection can also be measured as a function of the distance between the centers of the pump and probe spots, achieved by altering the incident angle of the probe beam by tilting the beamsplitter that reflects the probe. All the measurements were performed with the sample under ambient condition and at room temperature. Furthermore, no signs of sample degradation was observed during the entire course of the experiment.

RESULTS AND DISCUSSION

Figure 2(a) shows schematically the atomic structure of the monoclinic layered AsSbS₃. Each semimetal atom (As or Sb) is bond to three sulfur atoms to form a trigonal pyramidal. Eight such pyramidals connect into one octagon with each sulfur atom bonds to two semimetal atoms. The layered crystal structure is formed by these octagons *via* the van der Waals interlayer interaction.^{34,35}

The AsSbS₃ crystals used in this study were acquired from 2D Semiconductors. The bulk flakes of AsSbS₃ were fabricated by a standard mechanical exfoliation procedure using these crystals. An adhesive tape was used to cleave the crystal first to obtain a fresh surface. Another tape was then used to peel off flakes from the crystal onto a polydimethylsiloxane (PDMS) substrate. Large and uniform flakes were identified under an optical microscope, and then transferred onto a Si/SiO_2 substrate to facilitate optical measurements. Figure 2(b) shows an optical microscope image of one such flake. Atomic force microscope measurement was performed for the sample area indicated by the yellow square shown in Figure 2(b). The obtained height map is shown in (c), with a line scan (indicated by the white line) plotted in (d). According to this scan, the thickness of this flake is about 45 nm. From both optical and electronic aspects, such a thickness is large enough for the flake to be treated as a bulk sample. Figure 2(e) shows a Raman spectrum of this flake measured with a 532-nm laser. The broad Raman shift at about 300 cm⁻¹ is consistent with previous results, confirming

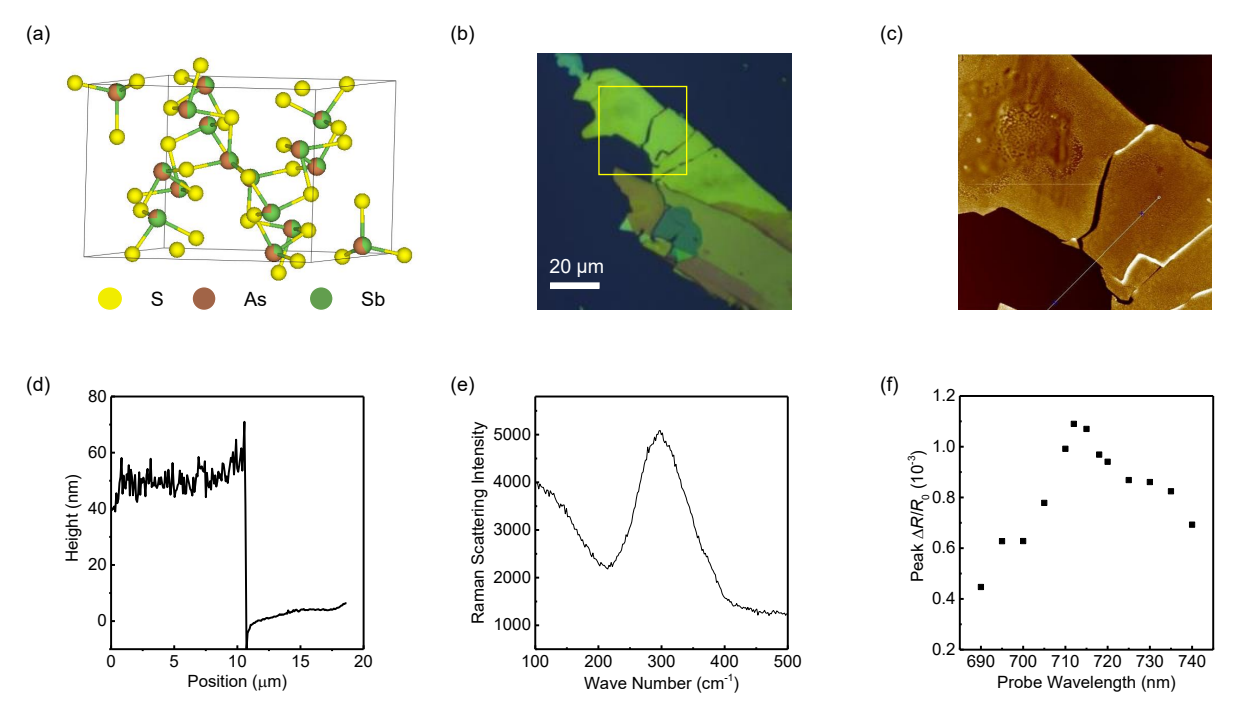


Figure 2: (a) Schematics of the lattice structure of $AsSbS_3$ layered crystal. (b) An optical microscope image of the $AsSbS_3$ sample exfoliated onto a Si/SiO_2 substrate. (c) The atomic force microscope image of the sample region indicated by the yellow square in (b). (d) Height profile of the sample along the white line shown in (c), which shows a sample thickness of about 45 nm. (e) Raman spectrum of the sample measured by using a 532-nm laser. (f) Peak differential reflection signal as a function of the probe wavelength, measured with a 405-nm pump.

the quality of the sample.³⁶

The electronic bandstructure and optical properties of AsSbS₃ are largely unknown. We attempted photoluminescence spectroscopic measurements; however, no signal was detected. To probe its bandstructure, we performed differential reflection spectroscopic measurements over a large spectral range. In such measurements (see Experimental Methods), a 405-nm pump pulse with a fluence of about 100 μ J cm⁻² excited photocarriers in the sample. The peak differential reflection signal, obtained by choosing the probe delay when the signal is maximum, is measured as a function of the probe wavelength. The result of one of such measurements is plotted in Figure 2(f). A peak at about 712 nm is observed. Since it is known that the differential reflection signal peaks when the probe resonates with the direct optical bandgap, ³³ this result identifies a direct bandgap of AsSbS₃ of about 1.74 eV.

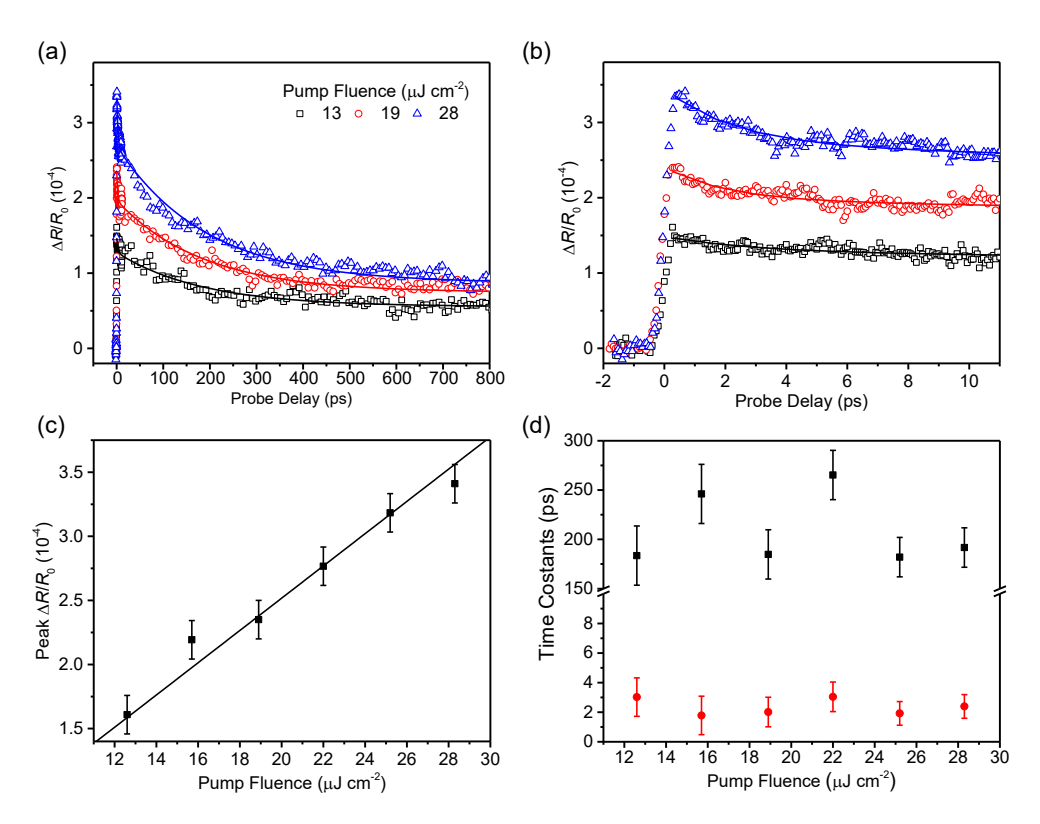


Figure 3: (a) Examples of the differential reflection signal as a function of the probe delay measured with a 405-nm pump and a 712-nm probe, under various pump fluences as indicated. The solid curves are biexponential fits (see text). (b) Same as (a) but over a shorter time range. (c) The peak differential reflection signal as a function of the pump fluence. The solid line is a linear fit. (d) The two time constants deduced from biexponential fits as a function of the pump fluence.

We next performed time-resolved differential reflection measurements, utilizing this direct transition, to study the photocarrier dynamics. The 405-nm pump, with a photon energy of 3.06 eV, excites photocarriers by interband absorption. The differential reflection of the 712-nm probe pulse was measured as a function of the probe delay. Figure 3(a) shows a few examples of the time-dependent differential reflection signal measured with different values of pump fluence, as indicated in the figure. Panel (b) provides a closer view of the signal near the zero probe delay. The rising part of the signal is limited by the time resolution of this setup of about 0.3 ps. This indicates that the photocarriers injected by the pump induces the peak differential reflection of the probe on a time scale shorter than the time resolution. The peak differential reflection is plotted as a function of the pump fluence in Figure 3(c).

The linear relation between the peak signal and the pump fluence, indicated by the line in the figure, confirms that the differential reflection can be used to monitor the photocarrier dynamics, since the injected photocarrier density is proportional to the pump fluence.

The decay of the signal can be satisfactorily fit by a bi-exponential function, $\Delta R/R_0 = A_1 \exp(-t/\tau_1) + A_2 \exp(-t/\tau_2) + B$, as shown by the solid curves in the Figure 3(a). The two time constants obtained from these fits are summarized in Figure 3(d). Both time constants are independent of the pump fluence. The long time constant of about 200 ps is attributed to the lifetime of the photocarriers. This value is on the same order of magnitude of most layered semiconductors, such as bulk MoS₂. This value is on the same order of magnitude of most layered semiconductors, such as bulk MoS₂. In a semiconductor, a low photoluminescence quantum yield can be caused by a short photocarrier lifetime (due to low crystalline quality) or the lowest bandgap being indirect in momentum space. Since the observed lifetime is moderate, the lack of photoluminescence signal suggests that AsSbS₃ is an indirect semiconductor. The pump-fluence-independent lifetime indicates that contributions from multiple-carrier processes 38,39 are negligible in the fluence range studied here. The short time constant of about 2 ps is also independent of the fluence. We can attribute this decay component to the energy relaxation of photocarriers from the states associated with the direct bandgap to those of the indirect bandgap. Such intervalley scattering decreases the differential reflection of the probe, which is tuned to the direct transition.

Finally, we performed spatially and temporally resolved differential reflection measurements to study the in-plane photocarrier transport properties. The spatial scans were achieved by changing the incident angle of the probe beam by tiling the beamsplitter that reflects it to the objective lens. At each probe position, the signal was measured as a function of the probe delay. Such scans produced the data plotted as the contour map in Figure 4(a). At each probe delay, the signal is a Gaussian function of the probe position. A few examples at various probe delays are shown as the symbols in Figure 4(b), along with the corresponding Gaussian fits (the curves). The rather symmetric profiles confirm that the setup was stable during the entire scan. Figure 4(c) shows the squared width (w^2) , where w

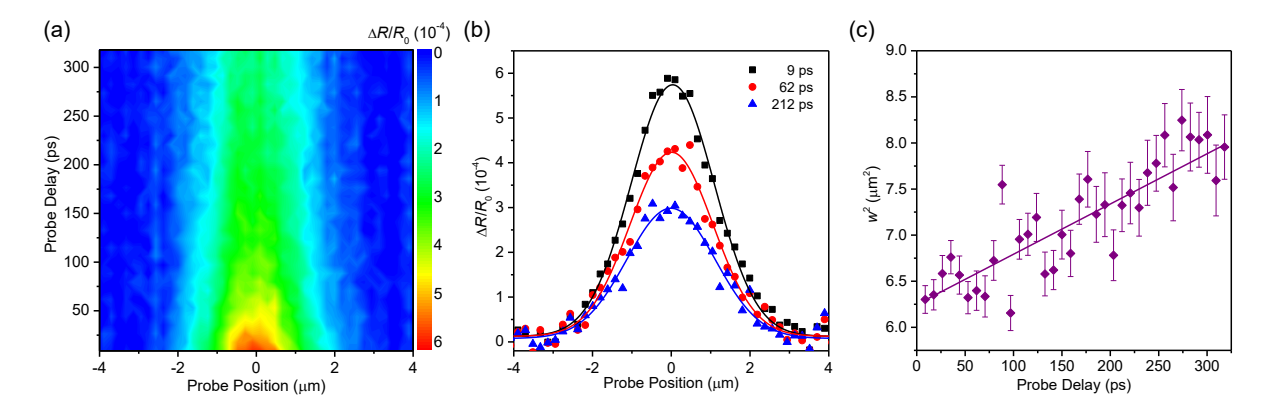


Figure 4: (a) Differential reflection signal as a function of the probe delay and probe position. (b) A few examples of the spatial profiles of the differential reflection signal (symbols) along with Gaussian fits (curves). (c) The squared width of the profiles as a function of the probe delay. The linear fit (solid line) produces a diffusion coefficient of 5 ± 1 cm² s⁻¹.

is the full width at half maximum) of the profile, obtained by the Gaussian fit, as a function of the probe delay.

The broadening of the profile over time is caused by the diffusion of the photocarriers after the excitation. Here, the major effect is the in-plane diffusion, since the interlayer diffusion occurs along the vertical direction and thus does not contribute to the lateral broadening of the profile. For an in-plane diffusion process, the classical drift-diffusion equation indicates that the squared width of the profile increases linearly with time,

$$w^{2}(t) = w_{0}^{2} + 16\ln(2)Dt, (1)$$

where w_0 and D are the initial width and the diffusion coefficient, respectively.³³ Based on this model, the data shown in Figure 4(c) was fit by a linear function, which results in a photocarrier diffusion coefficient of $D = 5 \pm 1$ cm² s⁻¹. Furthermore, using the photocarrier lifetime of about 200 ps shown in Figure 3(d), we obtain a photocarrier diffusion length of about 320 nm.

After the excitation, photocarriers can exist in forms of free electron-hole pairs or excitons. Currently, the properties of carriers in AsSbS₃ is largely unknown. If the exciton binding energy in AsSbS₃ is larger than the thermal energy at room temperature, photocarriers would be dominated by excitons, and the measured quantities would be the diffusion coefficient and diffusion length of excitons. Otherwise, these quantities would describe the ambipolar diffusion, where free electron-hole pairs diffuse as pairs due to their Coulomb attraction. Furthermore, by using the Einstein's relation, we can deduce an exciton or ambipolar mobility of $\mu = (D/e)k_BT$ of about 200 cm² V⁻¹ s⁻¹, where e, k_B , and T = 300 K, are the elementary charge, the Boltzmann constant, and the carrier temperature, respectively.

CONCLUSION

The vast interests and significant efforts since 2004 have created an extremely active research field on 2D materials. However, the 2D materials studied so far are still a small portion of the available layered materials. New layered materials that are suitable for 2D research are highly desired, especially since they can enrich the material library for fabricating 2D heterostructures. In this work, we showed that mechanical exfoliation can produce semiconducting nanofilms of AsSbS₃ that are stable under ambient conditions. Transient absorption spectroscopy identified a direct bandgap at about 712 nm, which is close to the ideal single-junction photovoltaic bandgap. Transient absorption microscopy measurements further revealed a photocarrier lifetime of about 200 ps, a diffusion coefficient of about 5 cm² s⁻¹, a diffusion length of about 320 nm, and a mobility of about 200 cm² V⁻¹ s⁻¹. These characteristics are comparable to previously studied 2D semiconductors, such as MoS₂. Hence, these results could stimulate more studies on this material and its potential integration with other 2D materials.

ACKNOWLEDGMENTS

We are grateful for the financial support of National Key R&D Program of China (2016 YFA0202302), National Natural Science Foundation of China (61527817, 61875236, 61905010,

61975007), Beijing Natural Science Foundation (Z190006), and U.S. National Science Foundation (DMR-1505852).

References

- (1) Novoselov, K. S.; Geim, A. K.; Morozov, S. V.; Jiang, D.; Zhang, Y.; Dubonos, S. V.; Grigorieva, I. V.; Firsov, A. A. Electric Field Effect in Atomically Thin Carbon Films. Science 2004, 306, 666–669.
- (2) Kim, K. S.; Zhao, Y.; Jang, H.; Lee, S. Y.; Kim, J. M.; Kim, K. S.; Ahn, J. H.; Kim, P.; Choi, J. Y.; Hong, B. H. Large-Scale Pattern Growth of Graphene Films for Stretchable Transparent Electrodes. *Nature* 2009, 457, 706.
- (3) Gibney, E. The Super Materials that Could Trump Graphene. *Nature* **2015**, *522*, 274–276.
- (4) Wang, Q. H.; Kalantar-Zadeh, K.; Kis, A.; Coleman, J. N.; Strano, M. S. Electronics and Optoelectronics of Two-Dimensional Transition Metal Dichalcogenides. *Nat. Nanotechnol.* 2012, 7, 699–712.
- (5) Lin, Z.; McCreary, A.; Briggs, N.; Subramanian, S.; Zhang, K. H.; Sun, Y. F.; Li, X. F.; Borys, N. J.; Yuan, H. T.; Fullerton-Shirey, S. K. et al. 2D Materials Advances: From Large Scale Synthesis and Controlled Heterostructures to Improved Characterization Techniques, Defects and Applications. 2D Mater. 2016, 3, 042001.
- (6) Freitag, M. Graphene: Trilayers Unravelled. Nat. Phys. 2011, 7, 596–597.
- (7) Splendiani, A.; Sun, L.; Zhang, Y.; Li, T.; Kim, J.; Chim, C. Y.; Galli, G.; Wang, F. Emerging Photoluminescence in Monolayer MoS₂. Nano Lett. **2010**, 10, 1271–1275.
- (8) Mak, K. F.; Lee, C.; Hone, J.; Shan, J.; Heinz, T. F. Atomically Thin MoS₂: A New Direct-Gap Semiconductor. *Phys. Rev. Lett.* **2010**, *105*, 136805.

- (9) Kumar, N.; Najmaei, S.; Cui, Q.; Ceballos, F.; Ajayan, P. M.; Lou, J.; Zhao, H. Second Harmonic Microscopy of Monolayer MoS₂. *Phys. Rev. B* **2013**, *87*, 161403.
- (10) Li, Y.; Rao, Y.; Mak, K. F.; You, Y.; Wang, S.; Dean, C. R.; Heinz, T. F. Probing Symmetry Properties of Few-Layer MoS₂ and h-BN by Optical Second-Harmonic Generation. *Nano Lett.* 2013, 13, 3329–3333.
- (11) Xiao, D.; Liu, G. B.; Feng, W.; Xu, X.; Yao, W. Coupled Spin and Valley Physics in Monolayers of MoS₂ and Other Group-VI Dichalcogenides. *Phys. Rev. Lett.* **2012**, *108*, 196802.
- (12) Zeng, H.; Dai, J.; Yao, W.; Xiao, D.; Cui, X. Valley Polarization in MoS₂ Monolayers by Optical Pumping. *Nat. Nanotechnol.* **2012**, *7*, 490–493.
- (13) Mak, K. F.; He, K.; Shan, J.; Heinz, T. F. Control of Valley Polarization in Monolayer MoS₂ by Optical Helicity. *Nat. Nanotechnol.* **2012**, *7*, 494–498.
- (14) Steinleitner, P.; Merkl, P.; Graft, A.; Nagler, P.; Watanabe, K.; Taniguchi, T.; Zipfel, J.; Schuller, C.; Korn, T.; Chernikov, A. et al. Dielectric Engineering of Electronic Correlations in a van der Waals Heterostructure. *Nano Lett.* 2018, 18, 1402–1409.
- (15) Chernikov, A.; Berkelbach, T. C.; Hill, H. M.; Rigosi, A.; Li, Y. L.; Aslan, O. B.; Reichman, D. R.; Hybertsen, M. S.; Heinz, T. F. Exciton Binding Energy and Nonhydrogenic Rydberg Series in Monolayer WS₂. Phys. Rev. Lett. 2014, 113, 076802.
- (16) He, K.; Kumar, N.; Zhao, L.; Wang, Z.; Mak, K. F.; Zhao, H.; Shan, J. Tightly Bound Excitons in Monolayer WSe₂. *Phys. Rev. Lett.* **2014**, *113*, 026803.
- (17) Yang, L. Y.; Sinitsyn, N. A.; Chen, W. B.; Yuan, J. T.; Zhang, J.; Lou, J.; Crooker, S. A. Long-Lived Nanosecond Spin Relaxation and Spin Coherence of Electrons in Monolayer MoS₂ and WS₂. Nat. Phys. 2015, 11, 830–834.

- (18) Radisavljevic, B.; Radenovic, A.; Brivio, J.; Giacometti, V.; Kis, A. Single-Layer MoS₂ Transistors. *Nat. Nanotechnol.* **2011**, *6*, 147–150.
- (19) Radisavljevic, B.; Kis, A. Mobility Engineering and a Metal-Insulator Transition in Monolayer MoS₂. Nat. Mater. **2013**, 12, 815–820.
- (20) Baugher, B. W. H.; Churchill, H. O. H.; Yang, Y.; Jarillo-Herrero, P. Optoelectronic Devices Based on Electrically Tunable P-N Diodes in a Monolayer Dichalcogenide. Nat. Nanotechnol. 2014, 9, 262–267.
- (21) Zhang, Y. J.; Oka, T.; Suzuki, R.; Ye, J. T.; Iwasa, Y. Electrically Switchable Chiral Light-Emitting Transistor. *Science* **2014**, *344*, 725–728.
- (22) Ross, J. S.; Klement, P.; Jones, A. M.; Ghimire, N. J.; Yan, J.; Mandrus, D. G.; Taniguchi, T.; Watanabe, K.; Kitamura, K.; Yao, W. et al. Electrically Tunable Excitonic Light-Emitting Diodes based on Monolayer WSe₂ P-N Junctions. *Nat. Nanotechnol.* 2014, 9, 268–274.
- (23) Pospischil, A.; Furchi, M. M.; Mueller, T. Solar-Energy Conversion and Light Emission in an Atomic Monolayer P-N Diode. *Nat. Nanotechnol.* **2014**, *9*, 257–261.
- (24) Geim, A. K.; Grigorieva, I. V. Van der Waals Heterostructures. *Nature* **2013**, 499, 419–425.
- (25) Liu, Y.; Weiss, N. O.; Duan, X.; Cheng, H.-C.; Huang, Y.; Duan, X. van der Waals Heterostructures and Devices. *Nat. Rev. Mater.* **2016**, *1*, 16042.
- (26) Novoselov, K. S.; Mishchenko, A.; Carvalho, A.; Neto, A. H. C. 2D Materials and van der Waals Heterostructures. *Science* **2016**, *353*, aac9439.
- (27) Mounet, N.; Gibertini, M.; Schwaller, P.; Campi, D.; Merkys, A.; Marrazzo, A.; Sohier, T.; Castelli, I. E.; Cepellotti, A.; Pizzi, G. et al. Two-Dimensional Materials from

- High-Throughput Computational Exfoliation of Experimentally Known Compounds. *Nat. Nanotechnol.* **2018**, *13*, 246–252.
- (28) Weissber, B. G. Getchellite AsSbS₃ a New Mineral from Numboldt County Nevada.

 Am. Mineral. **1965**, 50, 1817–1826.
- (29) Pertlik, F. Dimorphism of Hydrothermal Synthesized Copper Tellurite, CuTeO₃: The Structure of a Monoclinic Representative. J. Solid. State. Chem. **1987**, 71, 291–295.
- (30) Li, S.; Liu, Y.; Fu, B.; Yu, Z.-M.; Yang, S. A.; Yao, Y. Almost Ideal Nodal-Loop Semimetal in Monoclinic CuTeO₃ Material. *Phys. Rev. B* **2018**, *97*, 245148.
- (31) Cho, S.; Kim, S.; Kim, J. H.; Zhao, J.; Seok, J.; Keum, D. H.; Baik, J.; Choe, D. H.; Chang, K. J.; Suenaga, K. et al. Phase Patterning for Ohmic Homojunction Contact in MoTe₂. Science **2015**, 349, 625–628.
- (32) Keum, D. H.; Cho, S.; Kim, J. H.; Choe, D. H.; Sung, H. J.; Kan, M.; Kang, H.; Hwang, J. Y.; Kim, S. W.; Yang, H. et al. Bandgap Opening in Few-Layered Monoclinic MoTe₂. Nat. Phys. 2015, 11, 482–486.
- (33) Ceballos, F.; Zhao, H. Ultrafast Laser Spectroscopy of Two-Dimensional Materials beyond Graphene. *Adv. Funct. Mater.* **2017**, *27*, 1604509.
- (34) Guillermo, T. R.; Wuensch, B. J. Crystal-Structure of Getchellite, AsSbS₃. Acta Crystallogr. B **1973**, 29, 2536–2541.
- (35) Kyono, A.; Kimata, M. Structural Reinvestigation of Getchellite As_{0.98}Sb₁.02S_{3.00}. Am. Mineral. **2004**, 89, 696–700.
- (36) Lafuente, B.; Downs, R. T.; Yang, H.; Stone, N. In *Highlights in Mineralogical Crystal-lography*; Armbruster, T., Danisi, R. M., Eds.; De Gruyter: Berlin, Germany, 2015; pp 1–30.

- (37) Kumar, N.; He, J.; He, D.; Wang, Y.; Zhao, H. Charge carrier dynamics in bulk MoS₂ crystal studied by transient absorption microscopy. *J. Appl. Phys.* **2013**, *113*, 133702.
- (38) Kumar, N.; Cui, Q.; Ceballos, F.; He, D.; Wang, Y.; Zhao, H. Exciton-Exciton Annihilation in MoSe₂ Monolayers. *Phys. Rev. B* **2014**, *89*, 125427.
- (39) Sun, D.; Rao, Y.; Reider, G. A.; Chen, G.; You, Y.; Brezin, L.; Harutyunyan, A. R.; Heinz, T. F. Observation of Rapid Exciton-Exciton Annihilation in Monolayer Molybdenum Disulfide. *Nano Lett.* **2014**, *14*, 5625–5629.

Graphical TOC Entry

